



INCLUSIVE STRANGE PARTICLE PRODUCTION IN SINGLE-VEE EVENTS  
IN 200 GeV/c  $\pi^-$ N INTERACTIONS\*

S. Mikocki, J. R. Ficenec, S. Torres, and W. P. Trower  
Virginia Polytechnic Institute & State University, Blacksburg, VA 24061

and

T. Y. Chen, E. W. Jenkins, K-W. Lai, J. LeBritton, Y. C. Lin, and A. E. Pifer  
University of Arizona, Tucson, AZ 85721

and

H. C. Fenker and D. R. Green  
Fermi National Accelerator Laboratory, Batavia, IL 60510

and

J. R. Albright, J. H. Goldman, S. L. Hagopian,  
J. E. Lannutti, and J. E. Piper  
Florida State University, Tallahassee, FL 32306

and

C. C. Chang, T. C. Davis, R. N. Diamond, K. J. Johnson, and J. A. Poirier  
University of Notre Dame, Notre Dame, IN 46556

and

A. Napier and J. Schneps  
Tufts University, Medford, MA 02155

and

J. M. Marraffino, J. W. Waters, M. S. Webster, and E. G. H. Williams  
Vanderbilt University, Nashville, TN 37235

September 1985

Submitted to Physical Review D.



INCLUSIVE STRANGE PARTICLE PRODUCTION IN SINGLE-VEE EVENTS IN  
200 GEV/C  $\pi^-$ N INTERACTIONS

S. Mikocki<sup>a</sup>, J.R. Ficenece, S. Torres<sup>b</sup>, W.P. Trower  
Virginia Polytechnic Institute & State University,  
Blacksburg, Virginia 24061

T.Y. Chen<sup>Y</sup>, E.W. Jenkins, K-W. Lai, J. LeBritton<sup>d</sup>, Y.C. Lin<sup>e</sup>, A.E. Pifer  
University of Arizona, Tucson, Arizona 85721

H.C. Fenker, D.R. Green  
Fermilab, Batavia, Illinois 60510

J.R. Albright, J.H. Goldman, S.L. Hagopian, J.E. Lannutti, J.E. Piper<sup>z</sup>  
Florida State University, Tallahassee, Florida 32306

C.C. Chang<sup>n</sup>, T.C. Davis<sup>o</sup>, R.N. Diamond<sup>f</sup>, K.J. Johnson<sup>k</sup>, J.A. Poirier  
University of Notre Dame, Notre Dame, Indiana 46556

A. Napier, J. Schneps  
Tufts University, Medford, Massachusetts 02155

J.M. Marraffino, J.W. Waters, M.S. Webster, E.G.H. Williams<sup>l</sup>  
Vanderbilt University, Nashville, Tennessee 37235

(10 September 1985) \*

For the reaction  $\pi^- N + V^{\circ} X$ , where  $V^{\circ}$  is a  $K_S^{\circ}$ ,  $\Lambda$  or  $\bar{\Lambda}$  and  $X$  are charged particles, we measured the transverse and longitudinal momentum distributions, and inclusive cross sections for the  $V^{\circ}$  and for  $K^{*\pm}(892)$ ,  $\Sigma^{\pm}(1385)$  and  $\Xi^{\pm}(1321)$ . We compare our results with predictions of QCD quark counting rules.

Introduction: The hadron's constituent quarks and gluons in multiparticle production in soft collisions produce particular longitudinal momentum ( $X_F$ ) distributions of fast hadrons with low transverse momentum ( $P_T$ ) depending on the quark-parton models used.<sup>1</sup> One class of these models are the so-called quark counting rules (QCR). QCR predict the  $n$  of  $d_0/dX_F = A(1-X_F)^n$  for inclusive distributions observed in fragmentation processes as  $X_F \rightarrow 1$ , where  $n$  is interpreted as the number of spectator quarks involved. The exponent  $n$  differs if quark or gluon exchange is dominant or if the sea quarks are among the spectators, and depends on the details of how all this is accomplished.

The initially QCR predicted  $n = 2n_s - 1$ , where  $n_s$  is the least number of spectator valence and sea quarks from the beam hadron, which disagrees with experiment. Counting only valence quarks as spectators,  $n_s^V$ ,  $n = 2n_s^V - 1$ , which, although more successful, does not predict the observed baryon spectra steepness in meson fragmentation. QCR using lowest-order Quantum Chromodynamics (QCD) predict<sup>2</sup>  $n = 2n_H + n_{PL} - 1$ , where  $n_H$  is the number of initial hadron spectator quarks and  $n_{PL}$  is the number of spectators emerging from point-like bremsstrahlung interactions. These three QCR diagrams for  $\pi^- \rightarrow \Lambda$  are shown in Fig. 1.

Strange particle production in high-energy  $\pi$ -nucleon interactions requires that an additional quantum number pair be created whose dynamics provide information about the strong interactions. Further, strangeness can be a signature of charm production,<sup>3</sup> a subject of current interest.<sup>4</sup> Finally, new narrow resonances can be probed using a definite final state such as  $e^+e^-$  or  $\mu^+\mu^-$  ( $\rho, \omega, \phi, J/\psi, T$ ) whose spin-parity is restricted to  $J^P = 1^-$ . Different spin-parity states decay to two neutral strange particles, specifically  $K_S^0 K_S^0$  and  $\Lambda \bar{\Lambda}$ .

Thus motivated, the Fermilab Multiparticle Spectrometer (FMPS) experiment E580 was carried out in Spring 1980.<sup>5-9</sup> Here we report the analysis of events with only one reconstructed  $V^0$ . We first describe the FMPS, trigger and data analysis. We then report the production of strange particles [ $K_S^0$ ,  $\Lambda$ ,  $\bar{\Lambda}$ ,  $\Xi^-$ ,  $\bar{\Xi}^+$ ] and resonances [ $K^{*\pm}(892)$ ,  $\Sigma^\pm(1385)$ ], which we compare with QCR.

The Apparatus: Experiment E580 triggered on reactions  $\pi^- N \rightarrow V^0 V^0 X$  where  $V^0$  was a  $K_S^0$ ,  $\Lambda$  or  $\bar{\Lambda}$  while X were charged particles. The experiment was carried out with the FMPS, shown in Fig. 2, in the 200 GeV/c  $\pi^-$  M6W beam line. Not shown upstream of the target are two in-beam coincidence counters and an anticoincidence hole counter which defined the beam, and three proportional wire chamber (PWC) modules (BA1-3) which provided beam direction.

The active target was 20 individual ( $3.172 \pm 0.003$  cm<sup>2</sup> by  $0.621 \pm 0.006$  cm) plastic scintillators (Pilot-B with  $\rho \sim 1.032$  g/cm<sup>3</sup>). Each counter, wrapped in aluminum foil and heat shrink tubing, had a center-to-center spacing of 1.29 cm. For each trigger the pulse height of each counter was recorded.

Directly downstream of the target was the six PWC plane A station with two x(0°), two y(90°) and a u-v pair inclined at  $\pm 45^\circ$  to vertical. Downstream of the A station was a decay region, filled with helium gas to reduce interactions, where neutral strange particles decayed into charged tracks ( $V^0$ ). Next the five PWC plane B'-B station were in front of the spectrometer magnet. The superconducting ferrite magnet produced a 16.9 kG centrally homogeneous field at a maximum excitation of 180 A and had a 122(x) x 72(y) x 256(z) cm aperture and imparted a 697 MeV/c  $P_T$  change to each charged particle. Mounted directly upstream of the magnet pole piece was the C station with two PWC planes.

Downstream of the magnet was the five PWC plane D station whose u-v

pair was inclined at  $\pm 15^\circ$  to the vertical. Following was a nitrogen-filled, atmospheric pressure Cherenkov counter ( $C_B$ ) with 30 cells. Figure 3 shows the Cherenkov mirror segmentation while Table I summarizes its parameters. A small scintillation counter, S, was placed in the deflected beam line after the Cherenkov counter. Next were eight large magnetostrictive spark chamber modules, the E and F stations, constructed in two-gap units with stretched aluminum wire electrodes. Each unit had one gap with x electrodes and one formed with wires tilted at  $\tan \theta = \pm 0.1$  to the vertical. Each module with three magnetostrictive planes x, y and either u or v had a sensitive area of  $\sim 2.4 \times 1.2$  m (E) or  $\sim 3.6 \times 1.8$  m (F). Interspaced in the beam region of the F station were the F' station PWCs with a x-y pair and one v at  $45^\circ$ .

The Trigger: A defined beam particle and the absence of an S signal was an interaction. The trigger then counted the track hit clusters in  $A_U$  and  $A_V$  before, and  $B'_X$ ,  $B'_Y$ ,  $C_X$ ,  $C_Y$ ,  $D_X$ ,  $D_Y$  and  $D'_X$ , after, the decay volume. The  $V^0V^0$  trigger required a cluster multiplicity increase of  $4 \pm 1$  in the decay volume; multiplicity in at least two C and D planes equal to that measured in the B' station; and a primary cluster multiplicity measured before the decay volume of  $\leq 5$ . Up to three consecutive wire hits defined a cluster. Further, each target counter pulse height was summed to determine if the interaction had taken place there.

The Data: The average beam intensity was  $\sim 6 \times 10^5 \pi^-$  in a 1s spill over a 400 hour run which resulted in the total of  $1.2 \times 10^{10} \pi^-$  giving  $1.2 \times 10^6$   $V^0V^0$  triggers. An additional  $3 \times 10^5$  triggers of noninteracting beam, elastic scattering ( $1\pi$ ), diffractive ( $3\pi$ s) and  $V^0\pi$  events were taken for diagnostic purposes and to verify the mass and momentum scales.

All triggers were passed through a pattern recognition program, TEARS.

Noninteracting beam was used for momentum calibration, alignment and program tune-up. TEARS found straight track segments upstream and downstream of the magnet which were matched at the magnet midplane. Upstream segments which did not have hits in the A station were candidates for  $V^0$  decay legs. Loose cuts were made on the  $V^0$  mass and on the vertex in the decay volume.

Next, a global three-dimensional spline fit was made using a detailed magnetic field map to obtain momentum and angles for each track. Each  $V^0$  was tested with three hypotheses:  $K_S^0$ ,  $\Lambda$  and  $\bar{\Lambda}$ . For the best hypothesis the  $K_S^0$  mass distribution had a full width at half maximum (FWHM)  $14 \text{ MeV}/c^2$  while the  $\Lambda$  and  $\bar{\Lambda}$  distributions had  $5 \text{ MeV}/c^2$ . Finally, track parameters were varied in fits constrained to the  $V^0$  mass and decay vertex location, requiring the fit probability  $\geq 10^{-5}$ . Of the surviving  $\sim 70,500$   $V^0V^0$  events, 62% were  $K_S^0K_S^0$ , 16%  $K_S^0\Lambda$ , 13%  $K_S^0\bar{\Lambda}$ , 8%  $\Lambda\bar{\Lambda}$  and 1%  $\Lambda\Lambda$  or  $\bar{\Lambda}\bar{\Lambda}$ . Of the  $\sim 25\%$  of the  $\sim 230,000$  events where a single  $V^0$  was reconstructed 76% were  $K_S^0$ , 13%  $\Lambda$  and 11%  $\bar{\Lambda}$ .

The primary interaction vertex was found by two methods. In the first, all tracks, excluding beam and  $V^0$  tracks, were fitted to a point, requiring the chi-squared per degree of freedom,  $\chi^2/DF$ ,  $\geq 30$ . The poorest fitting track was deleted and the fit repeated. The vertex had to lie within  $5\sigma$  of the target boundaries. In the second method, the target ADCs were examined for abrupt pulse height increases, with up to three allowed. One such increase unambiguously gave the interaction vertex z-coordinate. Using the beam PWCs, the x and y track coordinates of the z interaction point were computed. When both methods gave a solution and the difference in their z-coordinates was greater than twice their summed z-coordinate errors, the direct track vertex was rejected. Otherwise, a weighted average of the two solutions was taken.

We then made cuts to eliminate false tracks found in pattern recognition as well as secondary interactions. We required that the primary vertex be  $\leq 5\sigma$  from the target boundaries and that the total visible momentum ( $V^0$  plus charged tracks)  $\leq 230$  GeV/c or we discarded the event. The  $V^0$  had to point to the primary vertex ( $\chi^2 < 20$ ); the decay vertex had to be  $\leq 3\sigma$  inside the decay region; and the  $V^0$  leg slope ( $\theta$ ) difference in the x-z (y-z) view had to be  $\Delta\theta_x \geq 0.5$  ( $\Delta\theta_y \geq 0.15$ ) mrad and leg intercept differences (b) had to be  $\Delta b_x \geq 0.15$  ( $\Delta b_y \geq 0.15$ ) cm or the  $V^0$  was discarded. Each charged track momentum had to be  $\leq 210$  GeV/c; have a  $\chi^2$  relative to the vertex of  $\leq 35$ ; and possess slope or intercept differences from  $V^0$  legs of  $\Delta\theta_x \geq 0.9$  ( $\Delta\theta_y \geq 0.4$ ) mrad or  $\Delta b_x \geq 0.25$  ( $\Delta b_y \geq 0.15$ ) cm, or the track would be discarded. Two primary tracks with slope and intercept differences  $\Delta\theta_x \leq 0.4$  ( $\Delta\theta_y \leq 0.25$ ) mrad and  $\Delta b_x \leq 0.20$  ( $\Delta b_y \leq 0.12$ ) cm resulted in one of the tracks being discarded. These cuts reduced the event sample to 25,565  $K_S^0$ , 3,999  $\Lambda$  and 3,041  $\bar{\Lambda}$ .

We study particle production by examining invariant mass distributions for given decay modes and fitting the  $X_F(dN/dX_F)$  or  $dN/dX_F = A(1-X_F)^n$  and  $(dN/dP_T^2) = B \exp(-b P_T^2)$  distributions. The backgrounds for these distributions are obtained from mass side-bands of the system under study. Only the  $X_F$  distributions are acceptance corrected using Monte-Carlo generated events for a given reaction with a flat  $X_F$  distribution and  $P_T^2$  distributed with  $b = 2.5$  (GeV/c) $^{-2}$  unless noted otherwise. These events were propagated through the FMPS using computer codes that take into account the detector geometry and the restricted  $V^0$  decay region. In performing the fits, the  $\chi^2$  contribution of each histogram bin is based on the difference between the number of events in the bin and the integral of the fitted function over that bin interval. The fits were obtained using a  $\chi^2$ -minimizing program (MINUIT) whose fit parameter error was determined by

an increase in  $\chi^2$  by one.

Particle Identification: Charged particle identification was made using the Cherenkov counter data with an identification algorithm<sup>10</sup> since the pion, kaon and proton momentum thresholds define four distinct momentum regions, as seen in Fig. 4. Tracks with momentum below threshold for pions that gave light could be electrons or could result from tracking or identification algorithm inefficiencies. Above the momentum for which protons should emit light, the small fraction where we observe no light we attribute to detector or algorithm inefficiency or to spurious tracks. We found the average particle identification inefficiency of ~20% by comparing Cherenkov assignments for known  $V^0$  leg masses. Ambiguous tracks involving pions we call pions and particles with momentum between 20.0 and 38.8 GeV/c which gave no light we call protons. For the analysis reported here particle identification was not used and all direct charged tracks we assumed were pions.

$K_S^0$  and  $K^*(892)$  Production: In Fig. 5 we plot the  $K_S^0 X_F$  distribution, where a fit over  $0.2 \leq X_F < 0.8$  gives  $n = 1.7 \pm 0.1$  with  $\chi^2/DF = 10/13$ . The QCR predict an  $A(1-X_F)^3 + B(1-X_F)^1$  dependence; this fit yields  $A/B = 1.7 \pm 0.1$  with 15/13.

The  $K_S^0 P_T^2$  distribution, shown in Fig. 6, is fit best by a sum of two exponentials with slopes  $2.1 \pm 0.3$  and  $5.0 \pm 0.5$  (GeV/c)<sup>-2</sup> while restricted  $X_F$  regions fit well to a single exponential with  $2.6 \pm 0.1$  ( $0.3 \leq X_F < 0.5$ ),  $2.7 \pm 0.1$  ( $0.5 \leq X_F < 0.7$ ) and  $3.1 \pm 0.3$  (GeV/c)<sup>-2</sup> ( $0.7 \leq X_F < 0.9$ ) showing that  $P_T^2$  increases with  $X_F$ . This increase would even be larger if these data were acceptance corrected.

The fits to the  $K_S^0 \pi$  invariant mass distribution, for  $X_F > 0$  and all  $P_T^2$ , are shown in Fig. 7. Although there is more  $K^{*-}(892)$  than  $K^{*+}(892)$  the  $K^*$

fraction in  $K_S^0 \pi$  is consistent for both charge states. We use a P-wave Breit-Wigner<sup>6</sup> for the  $K^*(892)$  and a background of  $A(M-m_0)^B \exp[-C(M-m_0) - D(M-m_0)^2]$ , where  $M$  is the  $K\pi$  mass,  $m_0$  the threshold mass and  $A$ ,  $B$ ,  $C$ ,  $D$  are fit parameters. The fitted mass ( $\text{MeV}/c^2$ ), full width at half-maximum ( $\text{MeV}/c^2$ ), number of events with  $\chi^2/\text{DF}$  is  $888 \pm 2$ ,  $64 \pm 8$ ,  $2,706 \pm 313$  with  $31/41$  for the  $K^{*-}$  and  $889 \pm 3$ ,  $70 \pm 12$ ,  $1,813 \pm 309$  with  $51/41$  for the  $K^{*+}$ . The  $K^{*0} X_F$  distribution, shown in Fig. 8, gives  $n = 0.9 \pm 0.2$  with  $\chi^2/\text{DF} = 3/2$  for  $K^{*-}$  and  $1.9 \pm 0.4$  with  $1/2$  for the  $K^{*+}$ . The  $X_F$  ratio, which is acceptance independent, gives  $n = 1.1 \pm 0.4$  and  $R(X_F=0) = 1.0 \pm 0.2$  with  $\chi^2/\text{DF} = 2/3$ .

The  $K^* P_T^2$  dependence fit, shown in Fig. 9, gives  $b = 2.7 \pm 0.3$  for  $K^{*-}$  and  $2.5 \pm 0.3$  ( $\text{GeV}/c$ )<sup>-2</sup> for  $K^{*+}$  for  $0 \leq P_T^2 \leq 1.2$  ( $\text{GeV}/c$ )<sup>2</sup> with  $\chi^2/\text{DF} = 13/4$  and  $11/4$ , respectively. The ratio of  $K^*$  to  $K_S^0$  is  $0.071 \pm 0.012$  and  $0.106 \pm 0.012$  for the  $K^{*+}$  and  $K^{*-}$ , respectively. If  $K^{*0}$  and  $\bar{K}^{*0}$  production is equal to  $K^{*+}$  and  $K^{*-}$ , then our  $R(K^*/K_S^0) \sim 0.35$  is consistent with bubble chamber experiments<sup>11</sup>.

$\Lambda$ ,  $\Xi(1321)$  and  $\Xi(1385)$  Production: In Fig. 10 we plot the  $\Lambda$  and  $\bar{\Lambda} X_F$  distributions which when fit for  $0.15 \leq X_F < 0.8$ , gives  $n = 2.0 \pm 0.1$  with  $\chi^2/\text{DF} = 7/11$  for  $\Lambda$  and  $2.0 \pm 0.1$  with  $12/11$  for  $\bar{\Lambda}$ . The  $R(\bar{\Lambda}/\Lambda) \sim 0.6$  at  $X_F \sim 0$  indicates target proton fragmentation. For  $0.1 \leq X_F < 0.65$ ,  $R(\bar{\Lambda}/\Lambda) \sim 0.8$ , and for  $X_F \geq 0.65$   $R(\bar{\Lambda}/\Lambda)$  increases above 1. This behavior was also seen in the  $K_S^0 \Lambda / K_S^0 \bar{\Lambda}$  data sample.<sup>7</sup>

A single exponential fit to the  $P_T^2$  distributions, shown in Fig. 11, for  $X_F > 0$  gives  $b = 2.5 \pm 0.1$  with  $\chi^2/\text{DF} = 19/22$  for  $\Lambda$  and  $2.6 \pm 0.1$  ( $\text{GeV}/c$ )<sup>-2</sup> with  $30/22$  for  $\bar{\Lambda}$ . For  $0.3 \leq X_F < 0.5$  and  $0.5 \leq X_F < 0.7$ , the slopes are  $2.6 \pm 0.2$  and  $2.3 \pm 0.3$  ( $\text{GeV}/c$ )<sup>-2</sup> for  $\Lambda$ , and  $2.4 \pm 0.2$  and  $2.1 \pm 0.4$  ( $\text{GeV}/c$ )<sup>-2</sup> for  $\bar{\Lambda}$ .

The  $\Xi(1321)$ , present in  $\Lambda\pi^-$  and  $\bar{\Lambda}\pi^+$  distributions, is shown in Fig. 12, where a fit to a Gaussian resonance with standard deviation  $\sigma$  and a quadratic background,  $A(M-m_0) + B(M-m_0)^2$ . This gives  $48 \pm 10$   $\Xi^-$  events with  $M$  and  $\sigma$  of  $1322.1 \pm 0.3$  and  $1.2 \pm 0.3$  MeV/c<sup>2</sup> and with  $\chi^2/DF = 76/75$ ; and  $33 \pm 10$   $\Xi^+$  events with  $1322.2 \pm 0.4$  and  $1.3 \pm 0.5$  MeV/c<sup>2</sup> with  $101/75$ . A fit to the combined distribution gives  $72 \pm 15$  events of  $1322.2 \pm 0.3$  and  $1.1 \pm 0.3$  MeV/c<sup>2</sup> with  $75/75$ . Our mass is slightly higher than the accepted<sup>3</sup>  $1321.52 \pm 0.13$  MeV/c<sup>2</sup> and our width is consistent with our mass resolution of  $1.5$  MeV/c<sup>2</sup> at the  $\Xi$  mass.

The  $X_F$  distributions, shown in Fig. 13, give  $n = 2.2 \pm 2.0$  for  $\Xi^-$  and  $8.4 \pm 9.0$  for  $\Xi^+$ . The  $P_T^2$  distributions, shown in Fig. 13, give  $b = 2.8 \pm 1.1$  and  $2.1 \pm 1.1$  (GeV/c)<sup>-2</sup> respectively, for  $\Xi^-$  and  $\Xi^+$ . In Fig. 14 we plot  $\Lambda\pi^-$  and  $\bar{\Lambda}\pi^+$  mass combinations and observe the  $\Xi(1321)$  and  $\Sigma(1385)$ . In Fig. 15,  $\Sigma^+(1385)$  is seen in  $\Lambda\pi^+$  but the  $\Sigma^-(1385)$  is only marginally present in  $\bar{\Lambda}\pi^-$ . We fit a Gaussian to the  $\Xi(1321)$ , a Breit-Wigner to the  $\Sigma(1385)$  and  $A(M-m_0)^B \exp[-C(M-m_0)^D]$  to the background, with masses fixed at the accepted values<sup>3</sup>. The  $\Xi(1321)$  widths were taken from the previous fits and the accepted  $\Sigma(1385)$  widths were increased by  $5$  MeV/c<sup>2</sup> to account for our mass resolution,  $\sigma = 2$  MeV/c<sup>2</sup> at the  $\Sigma$  mass. We get  $219 \pm 50$   $\Sigma^-(1385)$ ,  $154 \pm 46$   $\Sigma^+(1385)$ ,  $84 \pm 40$   $\bar{\Sigma}^-(1385)$  and  $64 \pm 42$   $\bar{\Sigma}^+(1385)$  events with a strange antibaryons-to-baryons ratio of  $\sim 0.4$ . Fits to the  $X_F$  and  $P_T^2$  distributions, seen in Fig. 16, for the more statistically significant  $\Sigma^-(1385)$  and  $\Sigma^+(1385)$  give  $n = 1.4 \pm 0.4$  with  $\chi^2/DF = 0.04/3$  and  $b = 3.9 \pm 2.4$  (GeV/c)<sup>-2</sup> with  $\chi^2/DF = 0.7/4$  for  $\Sigma^-(1385)$ , and  $n = 3.8 \pm 2.2$  with  $0.07/2$  and  $b = 2.9 \pm 1.4$  with  $1/4$  for  $\Sigma^+(1385)$ .

Comparison with QCR and Other Data: In Table II we summarize our fits to  $X_F$  distributions together with the predictions.<sup>2</sup> Our experimental  $n$

values, though systematically lower, are consistent with QCR except for  $K^{*+}$ . Since particles produced without a valence beam quark have a steeper  $X_F$  distribution than particles with the initial valence beam quark, we conclude that valence quarks play a significant role in strange particle production.

Recent E580 results<sup>9</sup> for  $K^*$  (892) from  $K_S^0 K_S^0 X$  data found  $n = 0.64 \pm 0.12$  for  $K^{*-}$ ;  $2.76 \pm 0.32$  for  $K^{*+}$ ; and  $R(K^{*+}/K^{*-}) = 0.89 \pm 0.19$  and  $n = 2.24 \pm 0.34$ .  $\bar{K}^{*0}$  and  $K^{*0}$  produced by 175 GeV  $\pi^-$  on beryllium<sup>12</sup> gave  $n = 0.69 \pm 0.10$  ( $0.1 \leq X_F \leq 0.9$ ) and  $0.59 \pm 0.13$  ( $0.3 \leq X_F \leq 0.9$ ) for  $K^{*0}$ ;  $1.82 \pm 0.27$  ( $0.1 \leq X_F \leq 0.9$ ) and  $1.47 \pm 0.51$  ( $0.3 \leq X_F \leq 0.9$ ) for  $\bar{K}^{*0}$ ; and  $R(\bar{K}^{*0}/K^{*0}) = 0.86 \pm 0.08$  and  $n = 1.11 \pm 0.27$ , consistent within errors to our  $R(K^{*+}/K^{*-})$  at  $X_F \sim 0$ .  $K^+$  and  $K^-$  production<sup>13</sup> gave for  $X_F < 0.5$   $n = 2.06 \pm 0.25$  for  $\pi^- \rightarrow K^-$  and  $2.85 \pm 0.22$  for  $\pi^- \rightarrow K^+$  at 175 GeV/c and similarly  $1.84 \pm 0.30$  and  $1.76 \pm 0.10$  at 100 GeV/c. The inclusive spectra from 200 GeV/c  $\pi^-$ -beryllium interactions<sup>10</sup> at  $P_T = 0$  gave  $n = 0.262 \pm 0.013$  for  $K_S^0$  and  $3.09 \pm 0.013$  for  $\Lambda$  and  $\bar{\Lambda}$ . The  $K_S^0$  and  $K^\pm$  distributions were intermediate between those of  $K^{*+}$  and  $K^{*-}$  values, as expected for significant resonance decay.

Strange baryon production<sup>7</sup> by  $\pi^-$  beam from the  $K_S^0 \Lambda / K_S^0 \bar{\Lambda}$  data gave  $n = 5.8 \pm 1.7$  for the combined  $\Sigma^\pm(1385) + \bar{\Sigma}^\pm(1385)$   $X_F$  distribution and  $6.7 \pm 0.3$  for  $\Xi^-(1321) + \bar{\Xi}^+(1321)$ . QCR predict  $n = 4$  for both fragmentation processes,  $K^- \rightarrow p$  and  $\pi^- \rightarrow \Sigma^+(1385)$ . From 100 and 175 GeV/c  $K^-$  data<sup>15</sup>  $n = 3.86 \pm 1.10$  for  $0.2 \leq X_F \leq 0.7$  and  $0.3 \leq P_T^2 \leq 1.0$  (GeV/c)<sup>2</sup> in agreement with our  $\Sigma^+(1385)$  value. Although QCR<sup>1</sup> reasonably estimate the  $n$  values, our data exhibits systematic differences between various processes of the same class, which is presumably related to spin and flavor effects.

Cross Sections: The cross section is defined as  $\sigma = SN_0/A'A$ .  $N_0$  is the number of observed events,  $A$  the spectrometer acceptance,  $A'$  a correction

for inefficiencies not included in the acceptance, and  $S$  the microbarn equivalent of the experiment (i.e. the cross section for 1 event) calculated as  $S = (N_t N_b)^{-1} = (32,800 \text{ events}/\mu\text{b})^{-1}$ , where  $N_t$  is the number of target particles,  $6.02 \times 10^{23}/\text{g} \times [12.80(\text{scint.}) + 0.548(\text{Al}) + 2.232(\text{tape})\text{g}/\text{cm}^2]$  or  $93.79 \times 10^{23}/\text{cm}^2$ , and  $N_b$  the effective (dead-time corrected) beam of  $3.5 \times 10^9$ . The experimental acceptance is a product of the probabilities that particles in an event will traverse the magnet and chambers (geometrical acceptance), the  $V^0$  will decay within decay region, the trigger will operate as designed (trigger efficiency), and the software will properly reconstruct the event. Included in 'A' is a correction for the branching fractions for a given decay mode and other corrections not included in A.

The experiment was designed to trigger on  $V^0 V^0$  events, so the trigger efficiency for  $V^0$  events should be substantially lower. True  $V^0$  events could satisfy the  $V^0 V^0$  trigger requirements if an interaction produced tracks between A and B' stations or if closely spaced multiple tracks formed one cluster in the A station, but not in the B station. Using different models for the trigger, we estimated that the trigger for  $V^0$  events was ~ 4 times lower than for  $V^0 V^0$  events. Independently,<sup>8</sup> it was found that the  $V^0 V^0$  trigger efficiency was  $0.40 \pm 0.04$ . The expected ratio of  $K_S^0 K_S^0$  to  $K_S^0$  events from measured bubble chamber cross sections<sup>16</sup> at 250 GeV/c using our estimated acceptances is  $0.29 \pm 0.16$ , in agreement with our experimental value  $0.255 \pm 0.003$ . Further, we compared the cross sections for the diffractive dissociation processes in the  $K_S^0 K_S^0$  and  $K_S^0$  samples.

In Table III we summarize the calculated partial cross sections for our observed states assuming a  $0.10 \pm 0.04$  trigger efficiency, a  $0.40 \pm 0.04$  software efficiency and current accepted branching fraction.<sup>3</sup> The geometrical and decay volume acceptances are estimated using Monte-Carlo

generated events for a given reaction. The partial cross section is trigger dependent and represents the forward cross section for the given state, with only one  $V^0$  in the final state and with low charge multiplicity. These cross sections are not inclusive cross sections because they do not contain events with more than one  $V^0$  or high charge multiplicity. To estimate the total inclusive cross sections for states decaying into  $V^0\pi^\pm$  we must determine our cross section normalization using those measured in a hydrogen bubble chamber<sup>17</sup> at 200 GeV/c:  $3.74 \pm 0.24$ ,  $1.53 \pm 0.12$  and  $0.43 \pm 0.06$  mb for  $K_S^0$ ,  $\Lambda$  and  $\bar{\Lambda}$ , respectively. We corrected for an additional observed pion by taking into account the relative acceptance  $V^0$  and  $V^0\pi$  for a given state. The total inclusive cross sections are given in Table III.

Other inclusive strange resonance production data in high energy  $\pi N$  interactions are limited. In 175 GeV/c  $\pi^-$  beryllium interactions,<sup>12</sup> the inclusive cross section ( $0.0 \leq X_F \leq 1.0$ ) is  $610 \pm 20 \pm 90$  and  $380 \pm 20 \pm 60 \mu\text{b}$  for  $K^{*0}(892)$  and  $\bar{K}^{*0}(892)$ , respectively. We conclude that there is no difference in  $\pi^-$  production of neutral and charged  $K^*(892)$ . For  $\pi^+p$  interaction<sup>11</sup> at 147 GeV/c the cross sections are  $1300 \pm 200 \mu\text{b}$  and  $700 \pm 200 \mu\text{b}$  for  $K^{*+}$  and  $K^{*-}$ , respectively, and are similarly  $1500 \pm 300$  and  $1200 \pm 300 \mu\text{b}$  for pp interactions.

The total inclusive cross sections for the  $K_S^0\Lambda/K_S^0\bar{\Lambda}$  sample<sup>7</sup> are  $41 \pm 4$  and  $23 \pm 8 \mu\text{b}$  for  $\Xi^- + \bar{\Xi}^+$  and  $\Sigma^{*\pm}(1385) + \bar{\Sigma}^{*\pm}(1385)$  production, respectively. In 147 GeV/c  $\pi^+p$  interactions,<sup>11</sup> the inclusive  $\Sigma^{*+}(1385)$  cross section is  $290 \pm 70 \mu\text{b}$  and  $\Sigma^{*-}(1385) < 100 \mu\text{b}$ . At the ISR<sup>18</sup> for  $X_F > 0.4$  the cross sections are 250, 40, and 9  $\mu\text{b}$  for  $\Sigma^+(1385)$ ,  $\Sigma^-(1385)$  and  $\Xi^-(1320)$ , respectively. However, they studied the proton fragmentation region, while we observe the forward hemisphere which includes the central and  $\pi^-$  fragmentation regions.

Our  $K^{*\pm}$  cross sections show an increase with beam energy and are consistent with other data. The  $\Xi^-$  cross section is consistent with low energy results assuming a logarithmic energy dependence. For  $\Sigma^{*\pm}$ , the low energy  $\pi^\pm$  cross sections increase with beam energy. Assuming similar trends as the  $\pi^+$  and p data show at higher energies, we expect the  $\Sigma^{*\pm}$  production cross sections to be  $\sim 300 \mu\text{b}$  at 200 GeV/c. Thus, our cross sections may be underestimated, or the  $\pi^-$  energy dependence is weaker than for other beams.

Diffractive Production: Diffractive dissociation, widely observed in hadroproduction, has been little studied for flavor dependence.<sup>19</sup> The diffractive  $\pi^-$  fragmentation<sup>6</sup> into  $K_S^0 K_S^0 \pi^+ \pi^- \pi^-$  ( $1.6 \pm 0.8 \mu\text{b}$ ) and  $K_S^0 K_S^0 \pi^-$  ( $3.4 \pm 1.0 \mu\text{b}$ ) give a cross section ratio of  $0.40 \pm 0.13$ , in agreement with 0.36 expected assuming the asymptotic topological cross section  $\sigma = C/N^2$ . C is a constant and N is the charged plus neutral multiplicity.

Using these results, we expect diffractive dissociation  $\pi^- \rightarrow K^0 K^- \pi^+ \pi^-$  and  $\bar{K}^0 K^+ \pi^- \pi^-$  cross sections of  $\sim 8-10 \mu\text{b}$ . To test this hypothesis we study the reaction  $\pi^- \rightarrow K_S^0 \pi^+ \pi^- \pi^-$  assuming that one pion is an unidentified kaon. Using 4,255  $K_S^0$  events with one positive and two negative primary tracks we isolate the diffractive component in the recoiling mass squared ( $MM^2$ ), shown in Fig. 17a, and interpret the peak at  $1 (\text{GeV}/c^2)^2$  as the recoiling target nucleon.

For exclusive reactions considerable effort is made to eliminate or correct for non-diffractive background. The shaded histogram in Fig. 17a shows the mass distribution recoiling against  $K_S^0 \pi^+ \pi^- \pi^-$ , where no similar low mass peak is expected or evident, since net positive charge final states can not be produced diffractively. To estimate the non-diffractive background in  $K_S^0 \pi^+ \pi^- \pi^-$  we fit a polynomial to the shaded histogram and normalize it to the unshaded histogram ( $203.5 \leq MM^2 \leq 273.5 (\text{GeV}/c^2)^2$ ) and

obtain the curve shown in Fig. 17b.

To correct for diffractive events with an unseen  $\pi^0$ , we assume that removing a  $\pi^0$  from  $K_S^0 \pi^+ \pi^- \pi^0$  is equivalent to removing the  $\pi^+$  from  $K_S^0 \pi^+ \pi^-$ . We therefore use the  $K_S^0 \pi^+ \pi^-$  events with  $MM^2 < 18.5 \text{ (GeV/c}^2\text{)}^2$ , throw out the  $\pi^+$ , calculate the  $K_S^0 \pi^- \pi^-$   $MM^2$  which we plot in Fig. 17c. Normalizing this histogram for  $23.5 \leq MM^2 \leq 273.5 \text{ (GeV/c}^2\text{)}^2$  to that in Fig. 17b and subtracting, we obtain Fig. 17d. The low mass peak FWHM is consistent with  $14 \text{ (GeV/c}^2\text{)}^2$ , the calculated spectrometer  $MM^2$  resolution. We assume that the  $304 \pm 30$  events with  $MM^2 < 18.5 \text{ (GeV/c}^2\text{)}^2$  are mostly single, with some double, diffractive events. To check this result, we fit the logarithmic-normal distribution plus polynomial background to the  $K_S^0 \pi^+ \pi^-$  distribution in Fig. 17e. In Fig. 17f we plot the fitted logarithmic-normal distribution (solid curve)<sup>20</sup> distribution after background subtraction and obtain  $300_{-22}^{+38}$   $K_S^0 \pi^+ \pi^-$  diffractive events with  $MM^2 < 18.5 \text{ (GeV/c}^2\text{)}^2$  in agreement with the first method.

To obtain the cross section we normalize our  $K_S^0$  sample to the  $1.41 \pm 0.28 \text{ mb}$  bubble chamber forward inclusive  $K_S^0$  production cross section.<sup>16</sup> Comparing the geometrical decay volume acceptances and trigger efficiencies for diffractive and all  $K_S^0$  events, we obtain  $\pi^- \rightarrow K^0 K^- \pi^+ \pi^-$  and  $\bar{K}^0 K^+ \pi^- \pi^-$ , single diffractive cross sections of  $11.2 \pm 5.9 \text{ } \mu\text{b}$  per channel, assuming that each channel contributes equally, in agreement with the expected value.

Summary: We studied the strange resonance production in  $\pi^- N$  interactions at 200 GeV/c with only one  $K_S^0$ ,  $\Lambda$  or  $\bar{\Lambda}$  in the final state. For  $K^*(892)$  production we find no difference between charged ( $K^{*-}, K^{*+}$ ) and neutral ( $K^{*0}, \bar{K}^{*0}$ ), but individually each is systematically produced more forward than QCR predict. A third of the  $K_S^0$  came from  $K^*$  decay. Strange baryon production is well predicted by QCR.  $\pi^- \rightarrow K^0 K^- \pi^+ \pi^-$  and  $\bar{K}^0 K^+ \pi^- \pi^-$

diffractive dissociation cross sections are consistent with fragmentation estimates.

We appreciate the assistance of R. Cantel and S. Hansen in preparing and running this experiment. Our work was supported by the Department of Energy (Arizona, Fermilab, Florida State, Tufts) and the National Science Foundation (Arizona, Notre Dame, Vanderbilt, Virginia Tech).

REFERENCES AND FOOTNOTES

- $\alpha$  Submitted in partial fulfillment for the Ph.D. degree.  
Present address: Undetermined.
- $\beta$  : Lab. Nazionali, Frascati (Roma) Italy.  
 $\gamma$  : Nanking University, Peoples Republic of China.  
 $\delta$  : Burr-Brown Research, Tucson AZ 85706.  
 $\epsilon$  : HEPL, Stanford CA 94305.  
 $\zeta$  : Planning Systems, Panama City FL 32401.  
 $\eta$  : AT&T Laboratories, West Longbranch NJ 07764.  
 $\theta$  : AT&T Laboratories, Naperville IL 60566.  
 $\int$  : American Dade, Costa Mesa, CA 92660.  
 $\kappa$  : Motorola, Tucson AZ 85721.  
 $\lambda$  : 61 Batten Hall, Worchester, United Kingdom.
1. P.D.B. Collins and A.D. Martin, Rep. Prog. Phys. 45, 335 (1983);  
and K. Fialkowski and W. Kittel, Rep. Prog. Phys. 46, 1283 (1983).
  2. J.F. Gunion, Phys. Lett. B88, 150 (1979).
  3. C.G. Wohl, et al., [Particle Data Group], Rev. Mod. Phys. 56, S1 (1984).
  4. A. Kernan and G. VanDalen, Phys. Rep. 106, 298 (1984).
  5. T.Y. Chen, et al., Phys. Rev. D28, 2304 (1983).
  6. C.C. Chang, et al., Phys. Rev. D29, 1888 (1984).
  7. H.C. Fenker, et al., Phys. Rev. D30, 872 (1984).
  8. E.G.H. Williams, et al., Phys. Rev. D30, 877 (1984).
  9. A. Napier, et al., Phys. Lett. B149, 514 (1984).
  10. S. Torres, Ph.D. Thesis, VPI, 1984.
  11. D. Brick, et al., Phys. Rev. D25, 2248 (1982).
  12. R. Bailey, et al., Z. Phys. C24, 111 (1984).
  13. A.E. Brenner, et al., Phys. Rev. D26, 1497 (1982).
  14. R.T. Edwards, et al., Phys. Rev. D18, 76 (1978).
  15. D. Cutts, et al., Phys. Rev. Lett. 43, 319 (1979).
  16. D. Bogert, et al., Phys. Rev. D16, 2098 (1977).
  17. N.N. Biswas, et al., Nucl. Phys. B167, 41 (1980).
  18. S. Erhan, et al., Phys. Lett. B85, 447 (1979).
  19. G. Alberi and G. Goggi, Phys.Rep. 74, 2 (1981); and K. Goulianos, Phys.Rep. 101, 174 (1983).

20. W.T. Eadie, D. Drijard, F.E. James, M. Roos, and B. Sadoulet, Statistical Methods in Experimental Physics, (North-Holland, Amsterdam, 1973).

Table I. Cherenkov  $C_B$  physical characteristics.

Dimensions	226 × 122 × 330 cm <sup>3</sup>
Mirror area	322 × 142 cm <sup>2</sup>
NTP gas	N <sub>2</sub>
Refractive index	1.0003
Radiator length	177 cm
Cone radius ( $\beta = 1$ )	4 cm
Number of mirrors	30
Mirror to target distance	8.7 m
Pion threshold	5.7 GeV/c
Kaon threshold	20.0 GeV/c
Proton threshold	38.8 GeV/c

Table II. Fits to  $(1-X_F)^n$  distributions.

Reaction	$X_F$	n	$\chi^2/DF$	n <sup>†</sup>
$\pi^- \rightarrow K_S^0$	0.2-0.8	1.7±0.1	10/13	1,3
$\rightarrow K^{*-}$	0.2-1.0	0.9±0.2	3/2	1
$\rightarrow K^{*+}$	0.2-1.0	1.9±0.4	1/2	3
$\rightarrow \Lambda$	0.2-0.8	2.0±0.1	7/11	2
$\rightarrow \bar{\Lambda}$	0.2-0.8	2.0±0.1	12/11	2
$\rightarrow \Sigma^{*-}$	0.0-1.0	1.4±0.4	0.04/3	2
$\rightarrow \Sigma^{*+}$	0.0-0.8	3.8±2.2	0.07/2	4
$\rightarrow \Xi^-$	0.0-1.0	2.2±2.0	1/2	2
$\rightarrow \Xi^+$	0.0-1.0	8.4±9.0	1/2	4

<sup>†</sup> from ref.2

Table III. The cross sections for observed states.

State	Observed events	Partial Cross-Section <sup>†</sup> [ $\mu\text{b}$ ]	Total Cross-Section <sup>††</sup> [ $\mu\text{b}$ ]
$K_S^0$	25,565 $\pm$ 160	109.1 $\pm$ 45.0	-
$\Lambda$	3,999 $\pm$ 63	22.6 $\pm$ 9.3	-
$\bar{\Lambda}$	3,041 $\pm$ 55	17.2 $\pm$ 7.1	-
$K^{*-}(892)$	2,706 $\pm$ 313	32.2 $\pm$ 13.8	1,103.5 $\pm$ 168.8
$K^{*+}(892)$	1,813 $\pm$ 309	21.6 $\pm$ 9.6	739.4 $\pm$ 146.0
$\Sigma^-(1385)$	219 $\pm$ 50	1.6 $\pm$ 0.7	105.2 $\pm$ 30.1
$\Sigma^+(1385)$	154 $\pm$ 46	1.1 $\pm$ 0.6	74.0 $\pm$ 25.5
$\Xi^-(1321)$	48 $\pm$ 10	0.5 $\pm$ 0.2	35.1 $\pm$ 9.5
$\Xi^+(1321)$	33 $\pm$ 10	0.4 $\pm$ 0.2	8.9 $\pm$ 3.0

<sup>†</sup> based on forward sensitivity  $S = (N_t N_b)^{-1} = (32,800 \text{ events}/\mu\text{b})^{-1}$  with associated low charged multiplicity.

<sup>††</sup> based on average normalization to the bubble chamber data.<sup>17</sup>

FIGURE CAPTIONS

- Figure 1. Fragmentation diagrams for  $\pi^- \rightarrow \Lambda$ .
- Figure 2. The experimental apparatus.
- Figure 3. Cherenkov mirror plane segmentation.
- Figure 4. Particle identification momenta regions.
- Figure 5. The  $K_S^0 X_F$  distribution.
- Figure 6. The  $K_S^0 P_T^2$  distributions.
- Figure 7. Mass spectra for  $K_S^0 \pi^\pm$ .
- Figure 8. The  $X_F$  distributions for (a)  $K^{*-}$  and  $K^{*+}$  and (b)  $R(K^{*+}/K^{*-})$ .
- Figure 9. The  $P_T^2$  distribution for  $K^{*-}$  and  $K^{*+}$ .
- Figure 10. The  $X_F$  distributions for (a)  $\Lambda$ , (b)  $\bar{\Lambda}$  and (c)  $R(\bar{\Lambda}/\Lambda)$ .
- Figure 11. The  $P_T^2$  distribution for (a)  $\bar{\Lambda}$  and  $\Lambda$ , (b)  $\Lambda$  and (c)  $\bar{\Lambda}$ .
- Figure 12. Mass spectra of  $\Xi(1321)$  region for (a)  $\Lambda\pi^\pm$ , (b)  $\Lambda\pi^-$  and (c)  $\bar{\Lambda}\pi^+$ .
- Figure 13. The  $X_F$  distributions for (a)  $\Xi^-$ , (b)  $\Xi^+$ ; and the  $P_T^2$  distributions for (c)  $\Xi^-$  and (d)  $\Xi^+$ .
- Figure 14. Mass spectra for (a)  $\Lambda\pi^-$  and (b)  $\bar{\Lambda}\pi^+$ .
- Figure 15. Mass spectra for (a)  $\Lambda\pi^+$  and (b)  $\bar{\Lambda}\pi^-$ .
- Figure 16. The  $X_F$  distribution for (a)  $\Sigma^{*-}$ , (b)  $\Sigma^{*+}$ ; and the  $P_T^2$  distributions for (c)  $\Sigma^{*-}$  and (d)  $\Sigma^{*+}$ .
- Figure 17. The analysis of diffraction production  $\pi^- \rightarrow K_S^0 \pi^+ \pi^- \pi^-$  explained in the text.

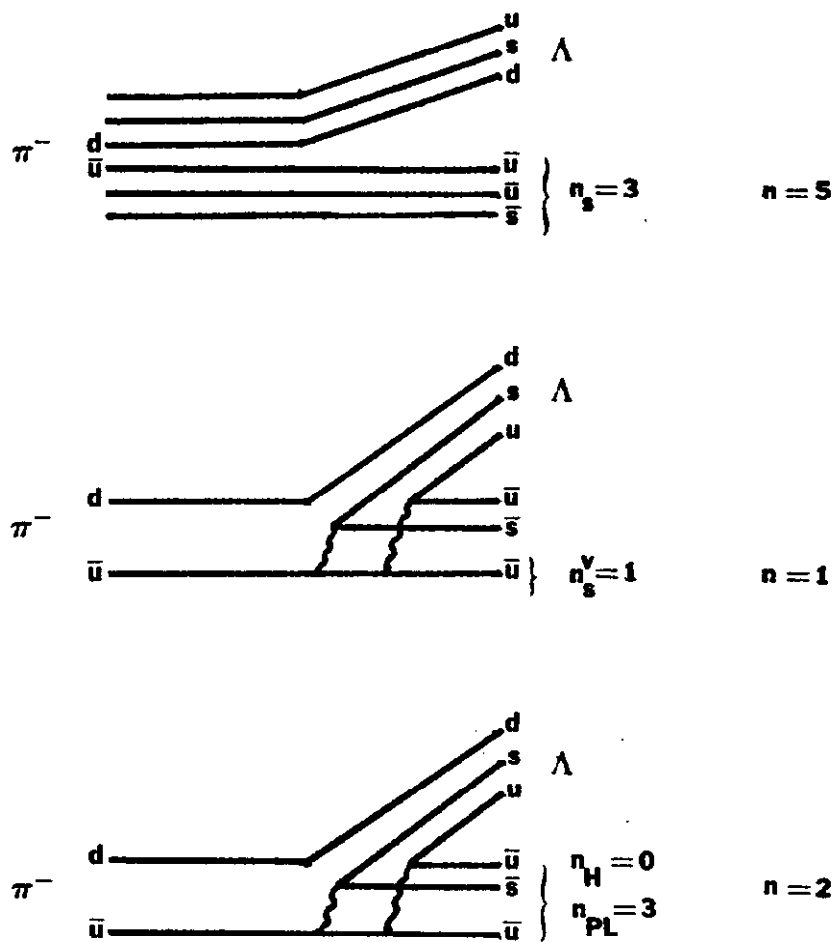


Fig. 1



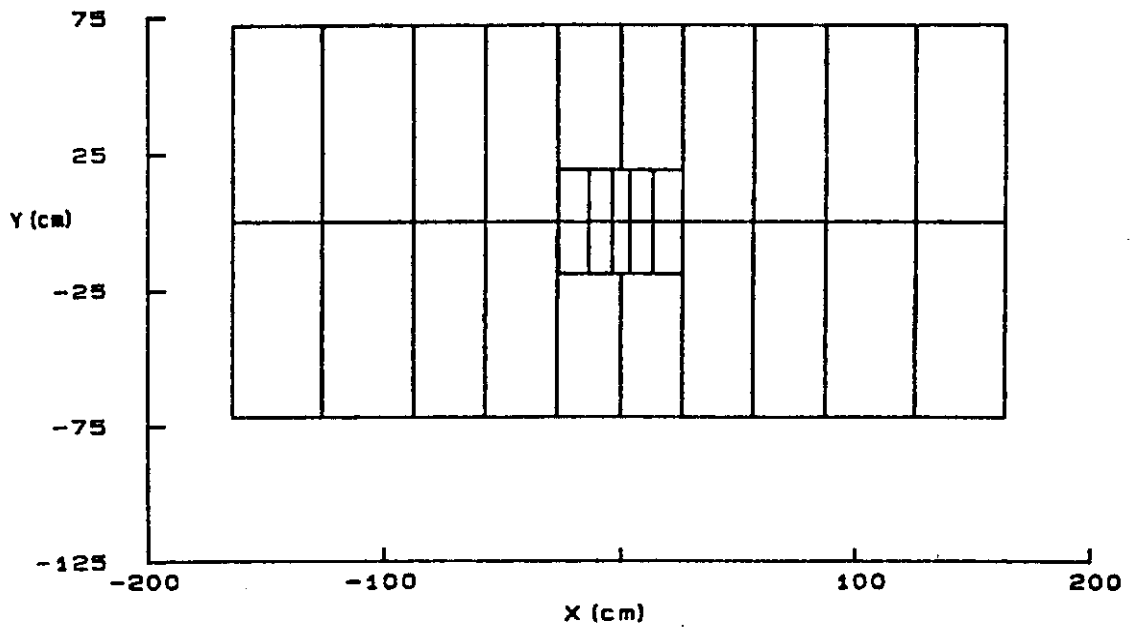


Fig. 3

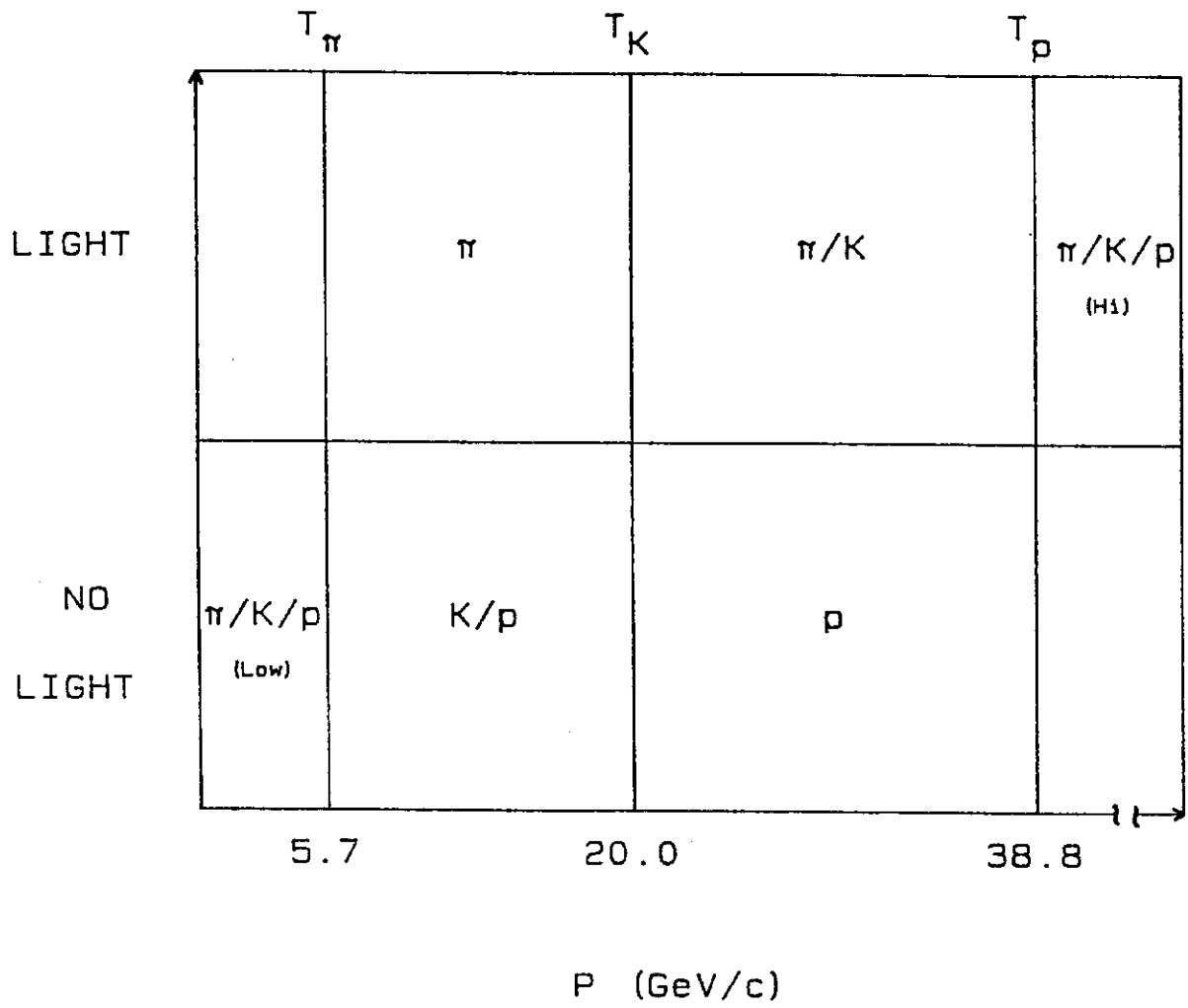


Fig. 4

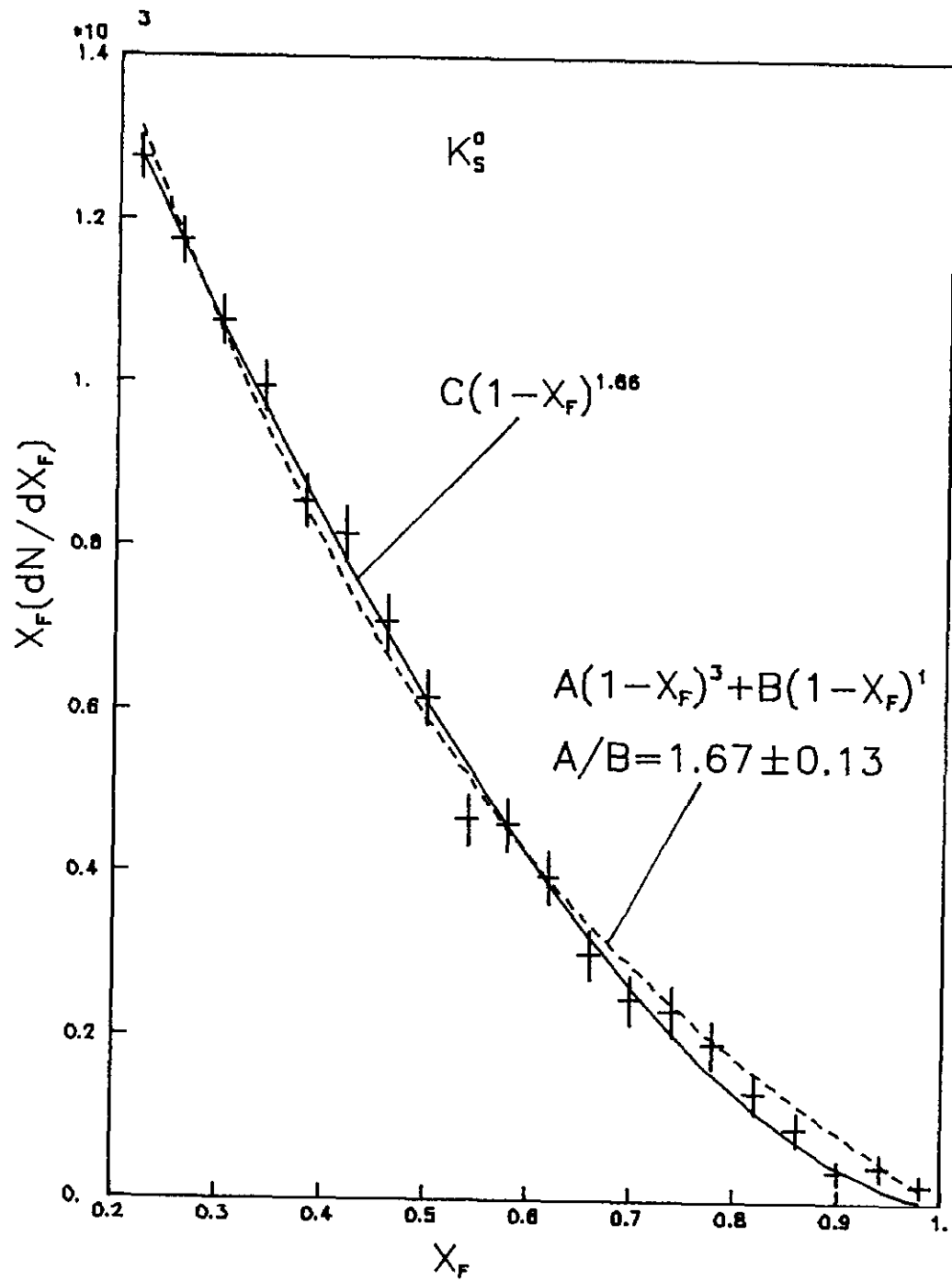


Fig. 5

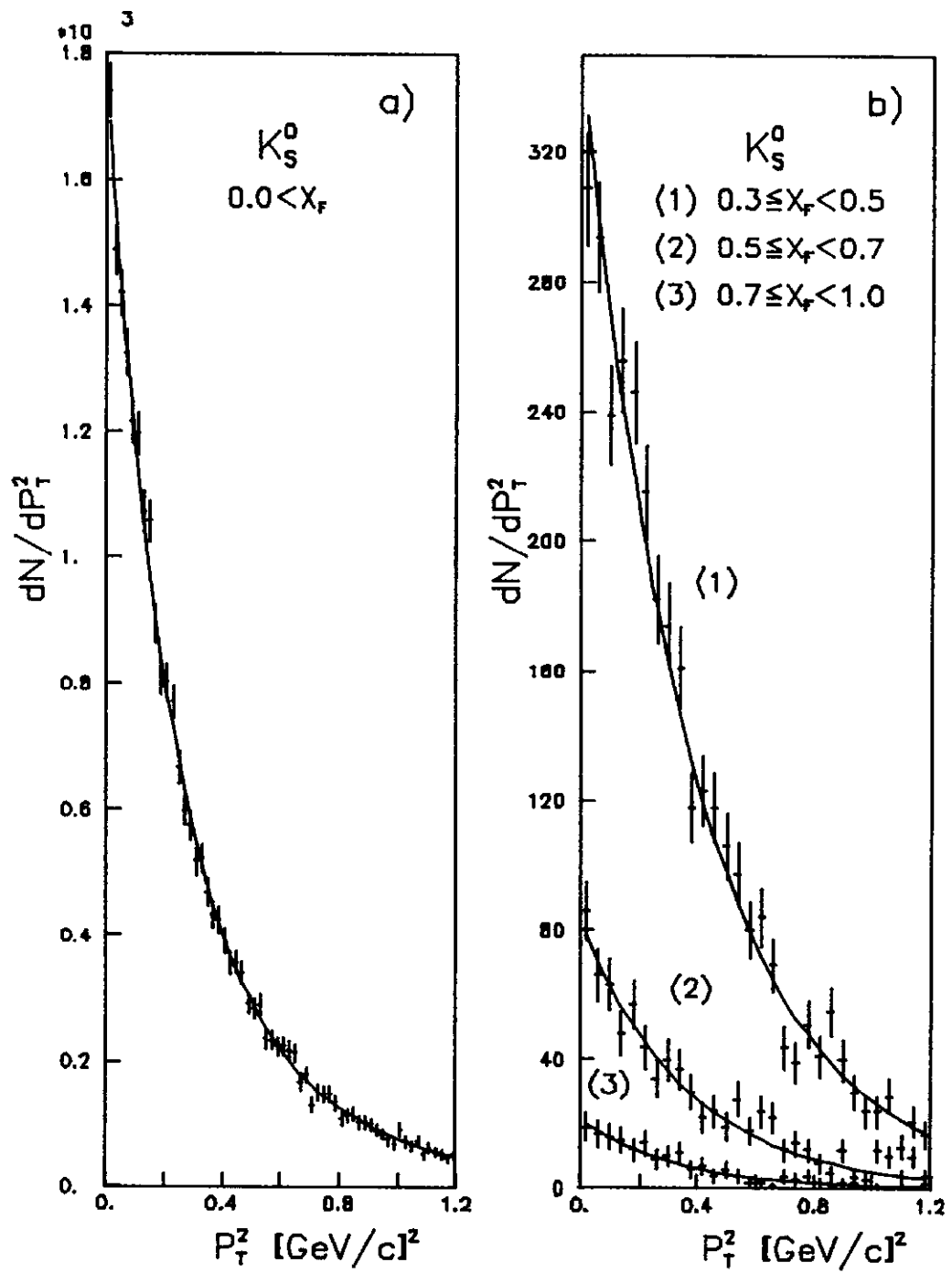


Fig. 6

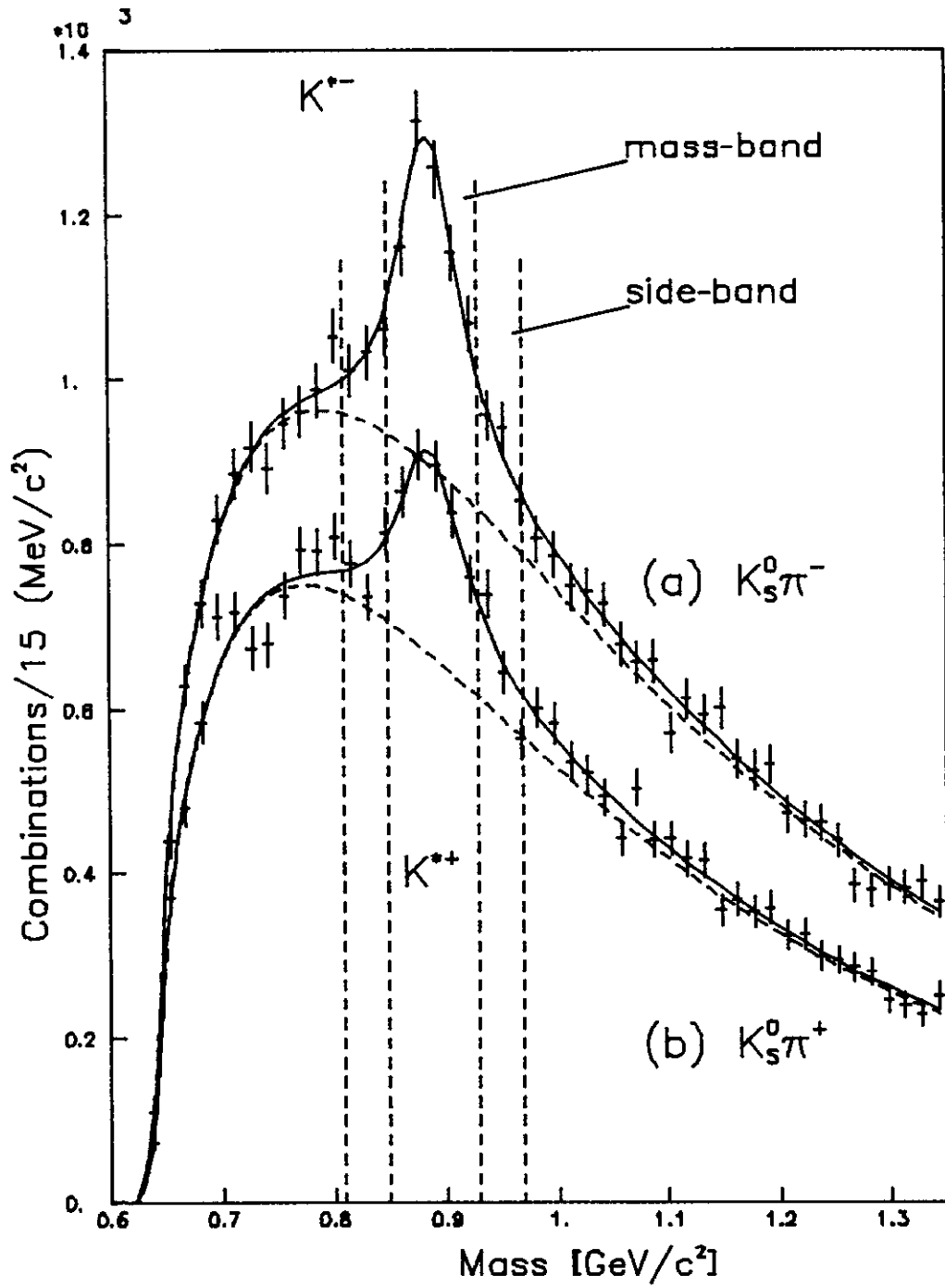


Fig. 7

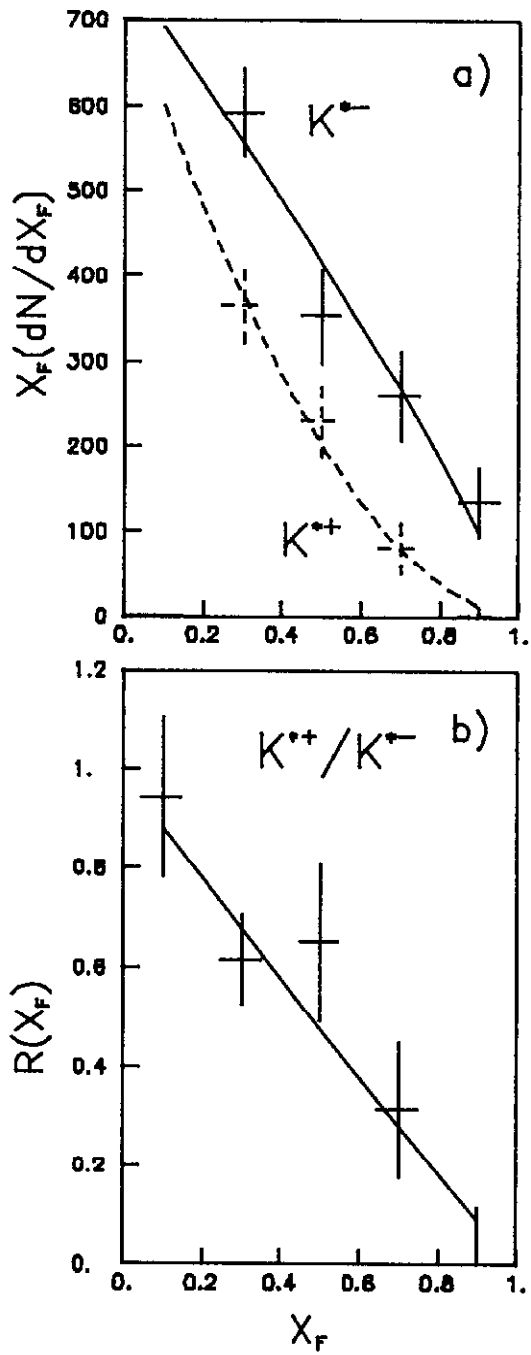


Fig. 8

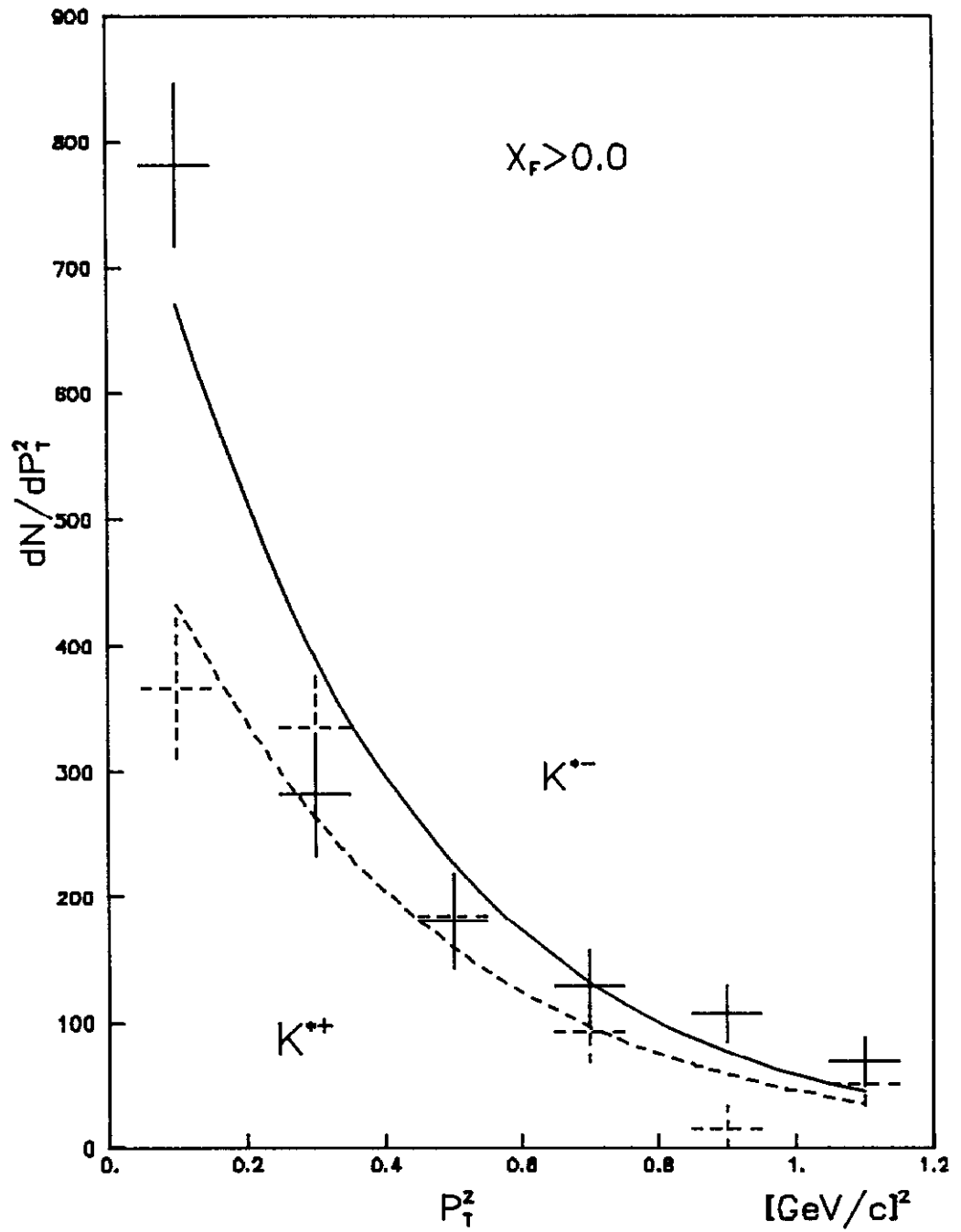


Fig. 9

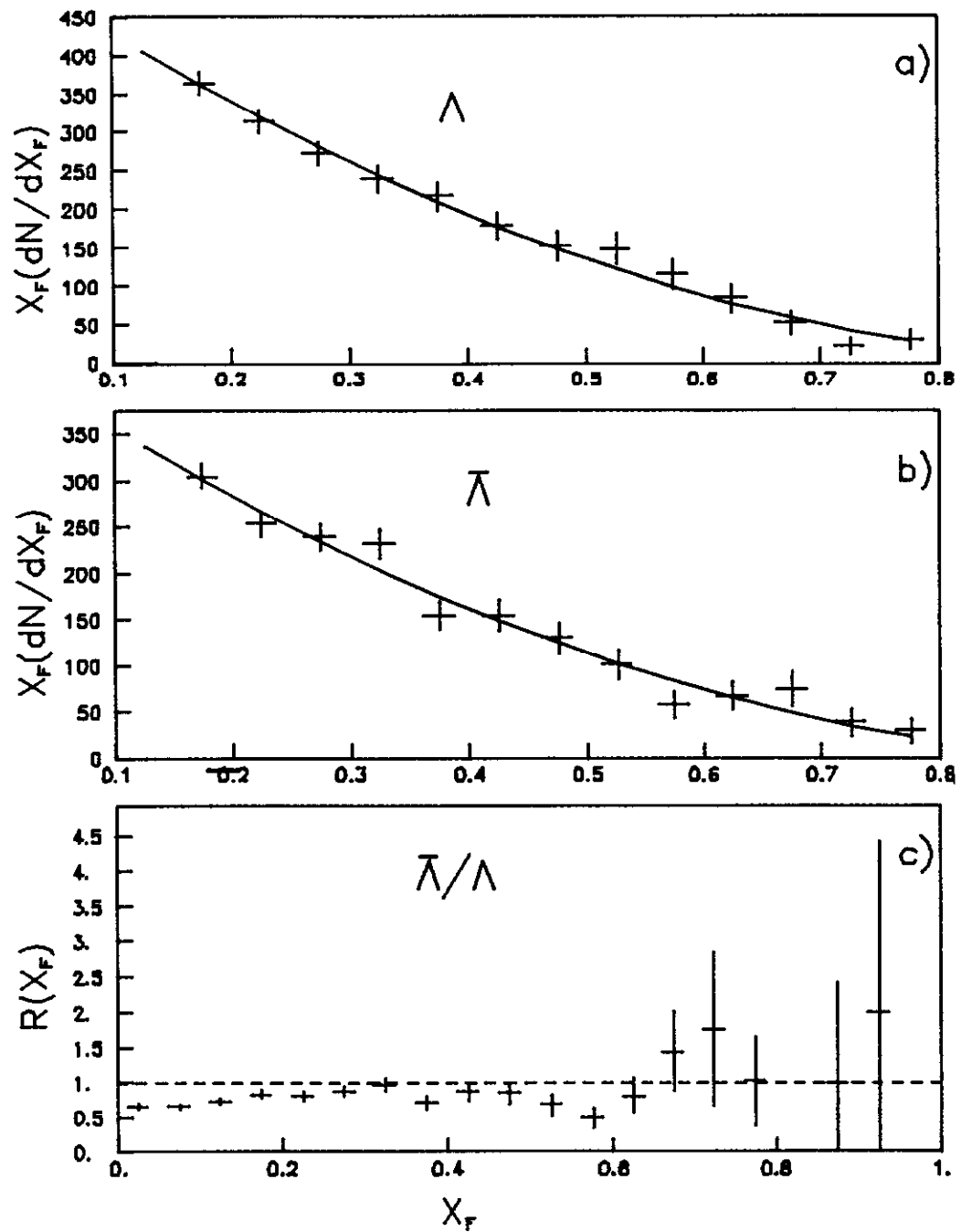


Fig. 10

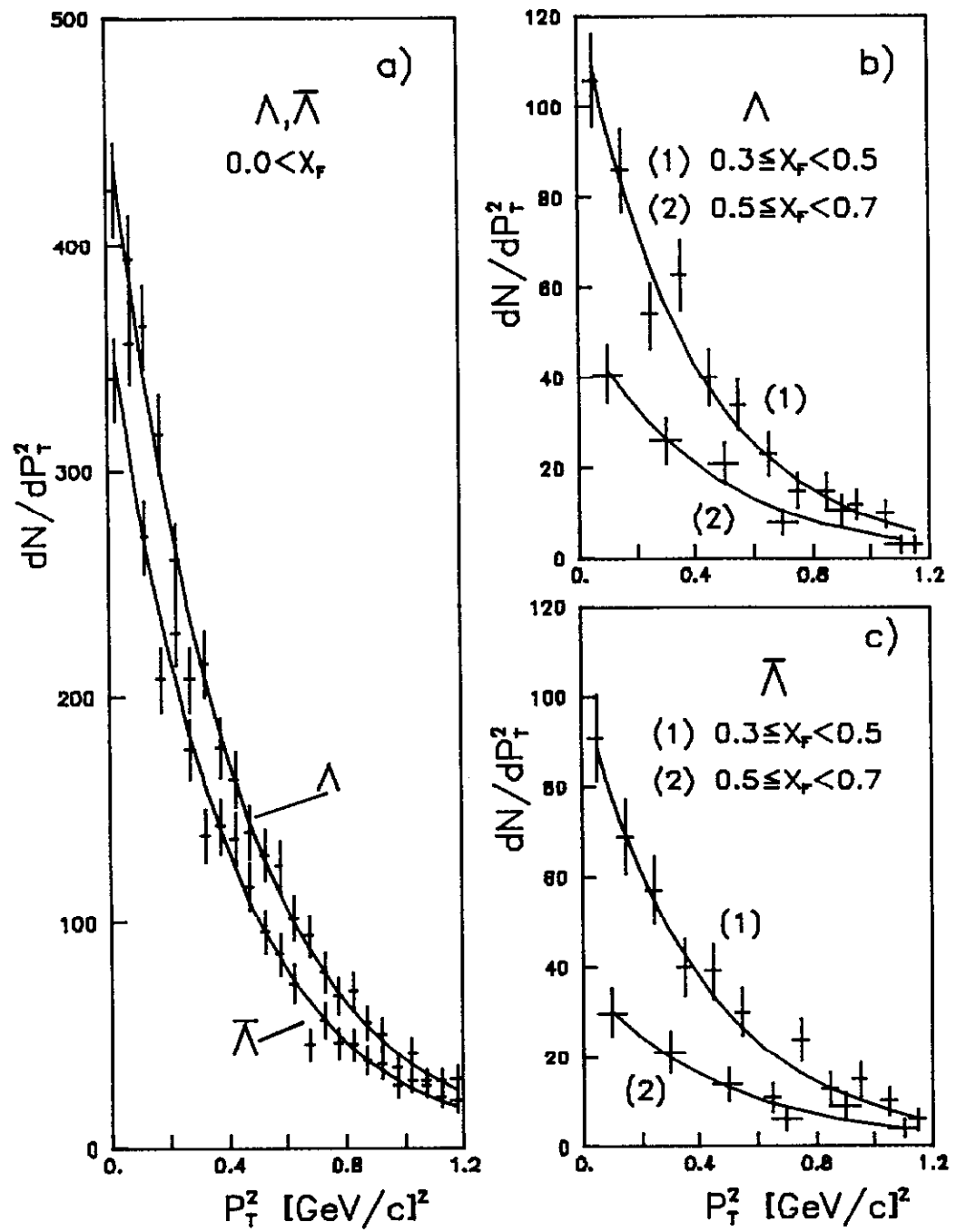


Fig. 11

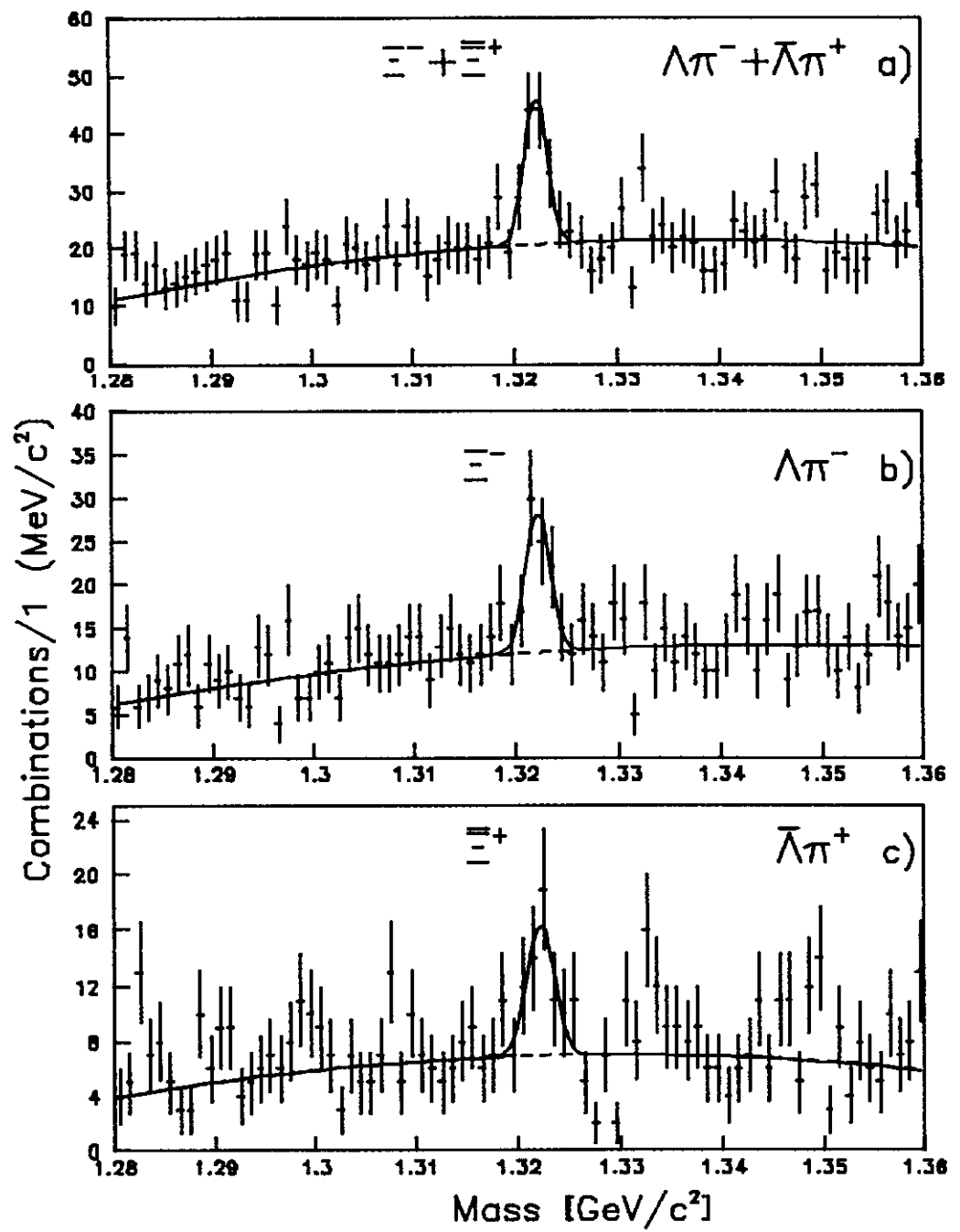


Fig. 12

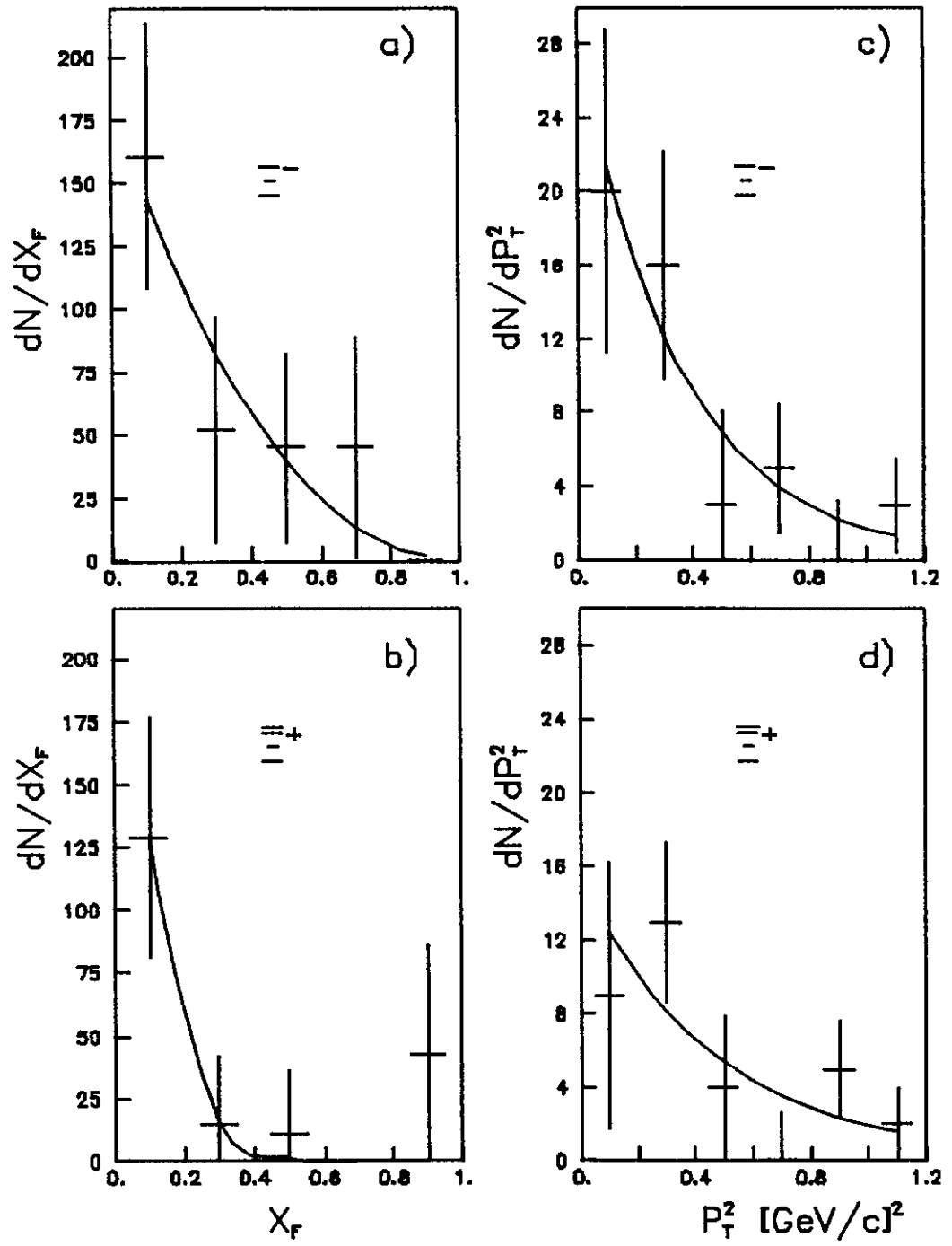


Fig. 13

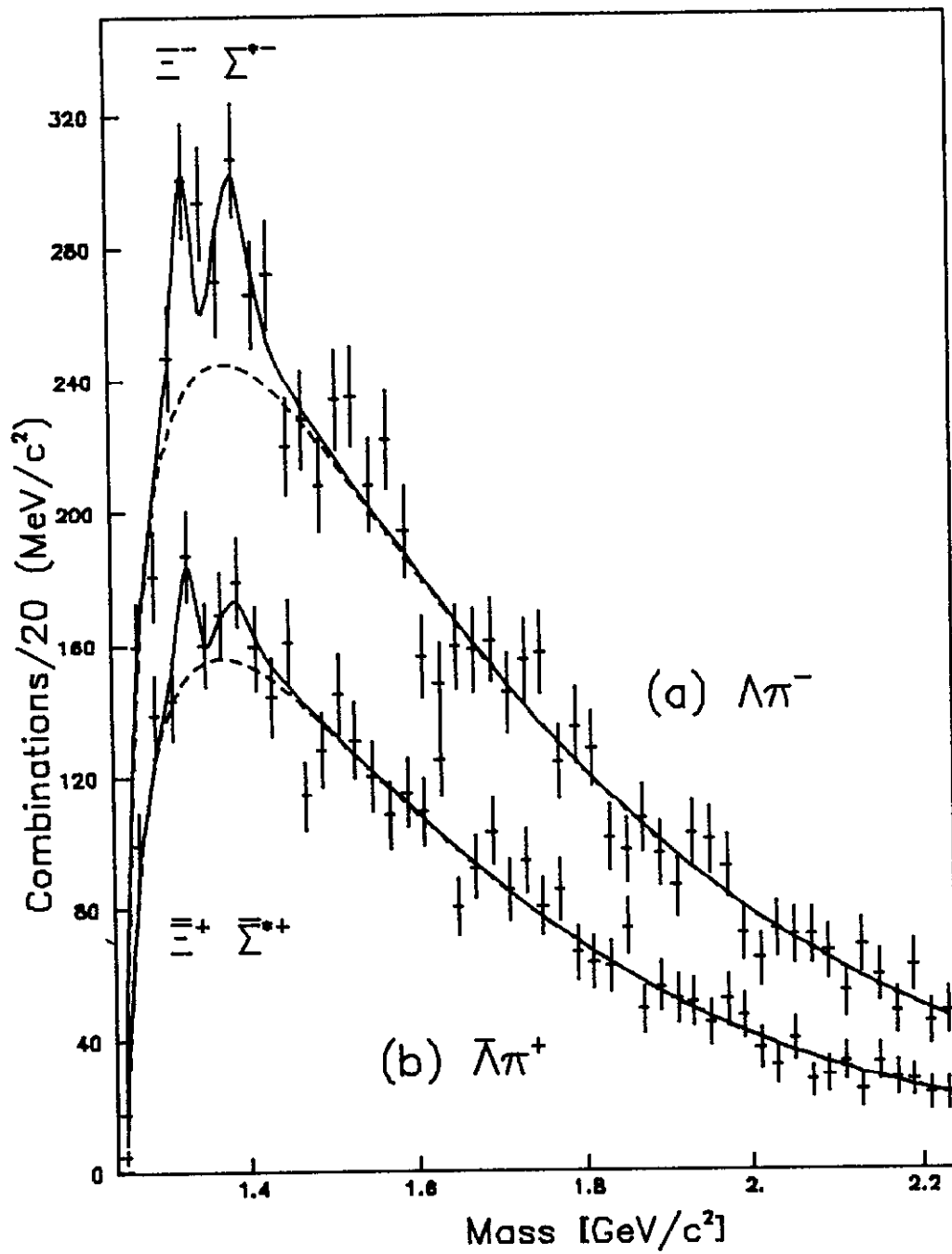


Fig. 14

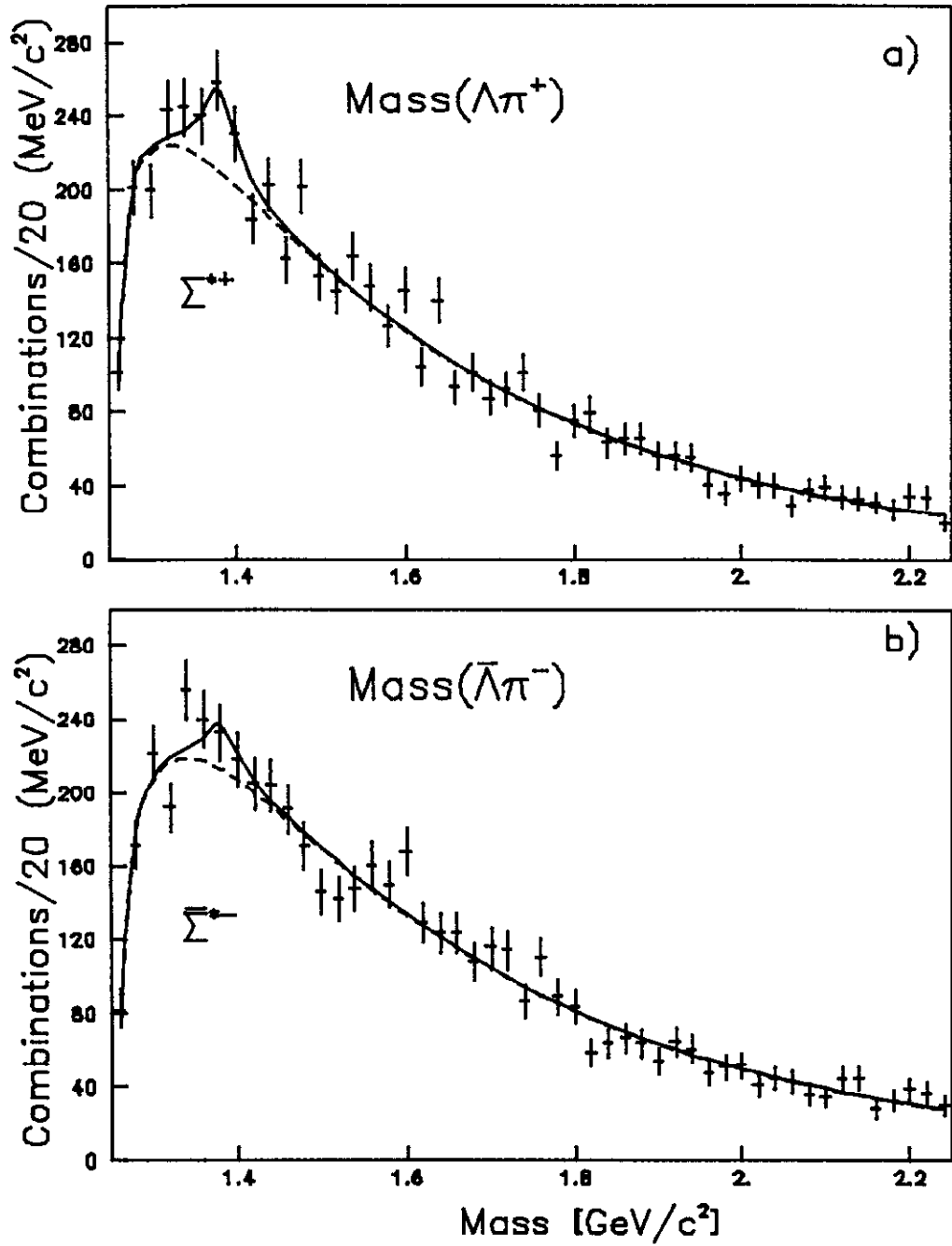


Fig. 15

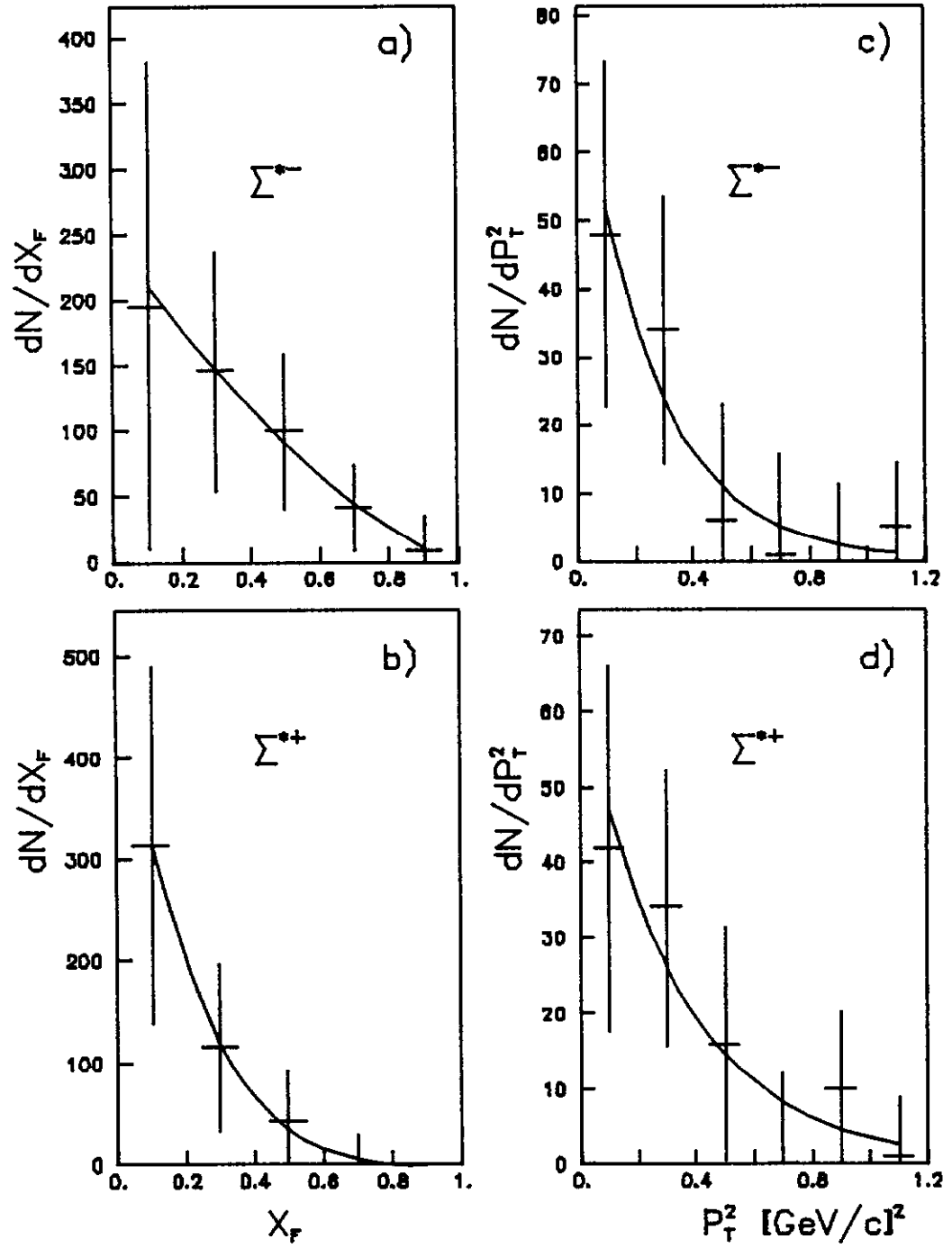


Fig. 16

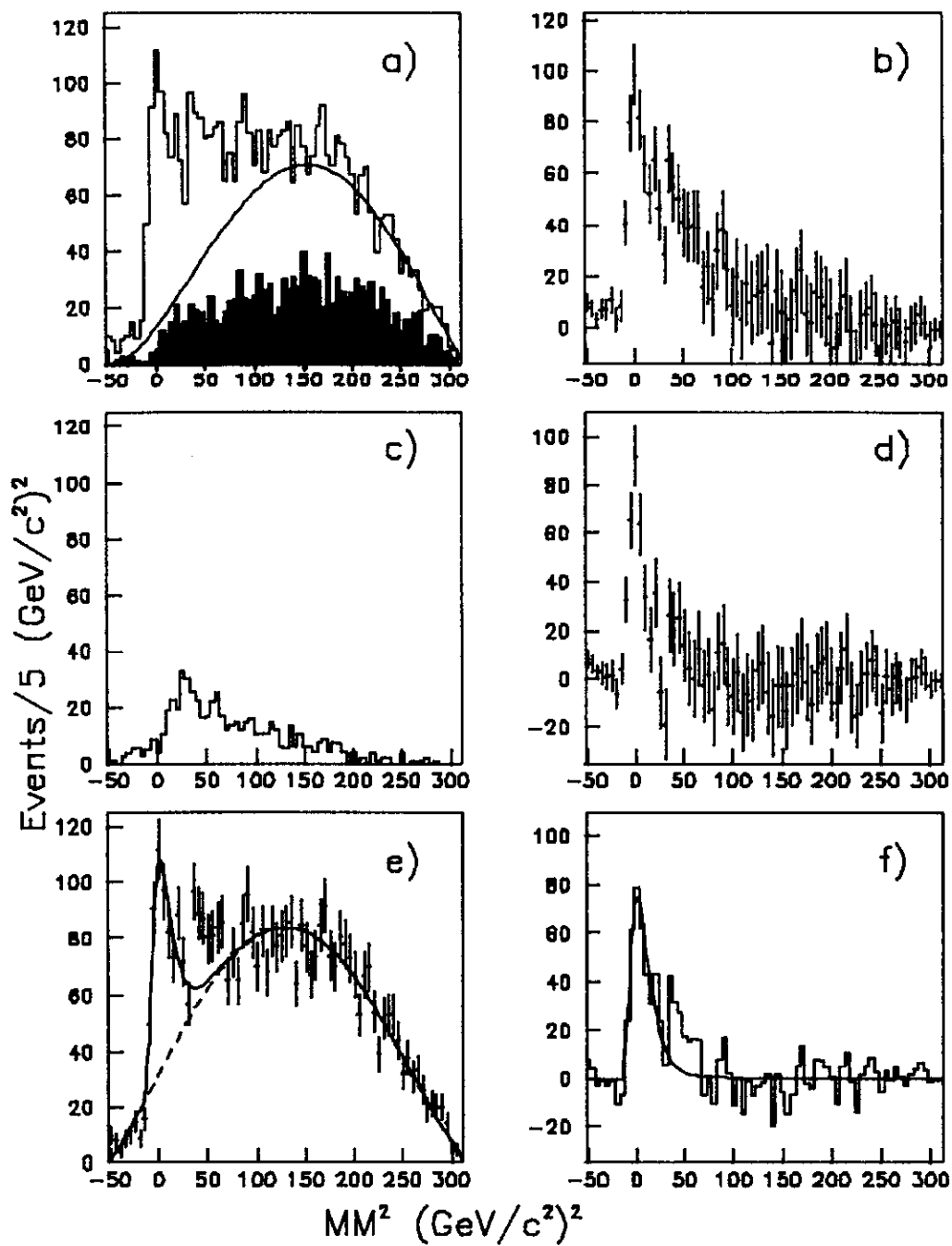


Fig. 17